NANO LETTERS
Letter
Cite This: Nano Lett. 2019, 19, 5036−5043
pubs.acs.org/NanoLett

Next-Generation Asymmetric Membranes Using Thin-Film Liftoff

Brian McVerry,[†,⊥] Mackenzie Anderson,[†,⊥] Na He,[†] Hyukmin Kweon,[‡] Chenhao Ji,[†] Shuangmei Xue,[†] Ethan Rao,[†] Chain Lee,[†] Cheng-Wei Lin,[†] Dayong Chen,[†] Dukwoo Jun,[†,‡] Gaurav Sant,[‡] and Richard B. Kaner*[,†,§,∥]

[†]Department of Chemistry and Biochemistry, University of California, Los Angeles, California 90095, United States
[‡]Department of Civil & Environmental Engineering, University of California, Los Angeles, California 90095, United States
[§]California NanoSystems Institute, University of California, Los Angeles, California 90095, United States
[∥]Department of Materials Science and Engineering, University of California, Los Angeles, California 90095, United States

Supporting Information

ABSTRACT: For the past 30 years, thin-film membrane composites have been the state-of-the-art technology for reverse osmosis, nanofiltration, ultrafiltration, and gas separation. However, traditional membrane casting techniques, such as phase inversion and interfacial polymerization, limit the types of material that are used for the membrane separation layer. Here, we describe a novel thin-film liftoff (T-FLO) technique that enables the fabrication of thin-film composite membranes with new materials for desalination, organic solvent nanofiltration, and gas separation. The active layer is cast separately from the porous support layer, allowing for the tuning of the thickness and chemistry of the active layer. A fiber-reinforced, epoxy-based resin is then cured on top of the active layer to form a covalently bound support layer. Upon submersion in water, the cured membrane lifts off from the substrate to produce a robust, freestanding, asymmetric membrane composite. We demonstrate the fabrication of three novel T-FLO membranes for chlorine-tolerant reverse osmosis, organic solvent nanofiltration, and gas separation. The isolable nature of support and active-layer formation paves the way for the discovery of the transport and selectivity properties of new polymeric materials. This work introduces the foundation for T-FLO membranes and enables exciting new materials to be implemented as the active layers of thin-film membranes, including high-performance polymers, two-dimensional materials, and metal−organic frameworks.

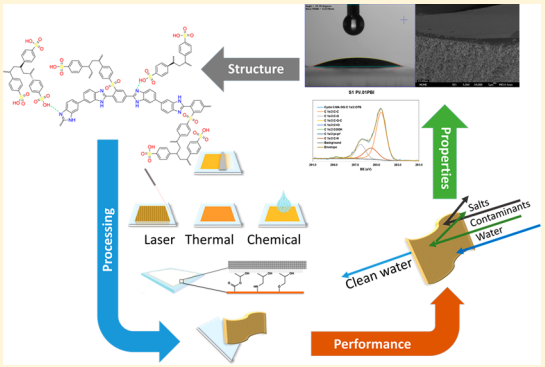

KEYWORDS: *thin film composite, membrane fabrication, reverse osmosis, nanofiltration, gas separation*

INTRODUCTION

Polymeric thin-film membranes have emerged as a leading technology for separations, because of their exceptional transport properties, large surface area/small footprint, and low cost of fabrication.[1] A major breakthrough in membrane technology occurred when Loeb and Sourirajan developed the first asymmetric membrane,[2] made from cellulose acetate (CA), that demonstrated superior permeation flux, when compared to dense CA membrane films.[3] Because the separation ability of a membrane is independent of its thickness,[4] a thin separation layer imparts higher permeability to a membrane, compared to a thick layer, while theoretically maintaining the same rejection capabilities.[5] To improve on this work, Cadotte et al. developed asymmetric thin-film composite (TFC) membranes with polyamide active layers made via interfacial polymerization.[6] Today, TFC membranes are the state-of-the-art technology used for nanofiltration, and brackish and seawater desalination. The pore sizes of these membranes can be readily tailored for different applications: membranes with larger pores are used in wastewater treatment and kidney dialysis (ultrafiltration) while nonporous membranes are used in nanofiltration, seawater desalination, and gas separation.

Despite their great performance, today's polymeric thin-film composite membranes have several limitations. Placing a thin active layer (∼150 nm) on top of a porous support membrane (typically made from polysulfone) is achieved using interfacial polymerization, which limits membrane precursors to highly reactive acyl chlorides and polyamines or polyols that react on contact.[7] Moreover, the rapid reaction rate of interfacial polymerization[8−18] leads to a rough active layer that creates sites that initiate membrane fouling.[19] Because the active layer is formed on the already made support membrane, the properties of the support membrane must be considered before forming the active layer. For example, solution casting of thin films onto a support membrane often causes issues with

Received: March 28, 2019
Revised: July 3, 2019
Published: July 5, 2019

DOI: 10.1021/acs.nanolett.9b01289
Nano Lett. 2019, 19, 5036−5043

dissolution of the support polymer or leads to poor lamination between the two layers. Many polymers known for their chlorine tolerance or pH stability must be thermally cured at higher temperatures than the support membrane can withstand, which limits the current curing conditions to relatively mild temperatures.[20]

In this contribution, we present a new thin-film liftoff (T-FLO) technique to fabricate robust thin-film composite membranes, which opens the door to the use of a variety of polymers and carbon materials as active layers. With T-FLO, an active layer precursor is first cast onto a substrate using a doctor blade to form a thin film, followed by solvent evaporation or curing. Next, a thermosetting resin is cast directly on top of the active layer and thermally cured to form a microporous support. As the support cures and hardens, the polymerization simultaneously generates covalent interactions with the active layer that enables the defect-free delamination of the active layer from the underlying substrate (Figure 1).

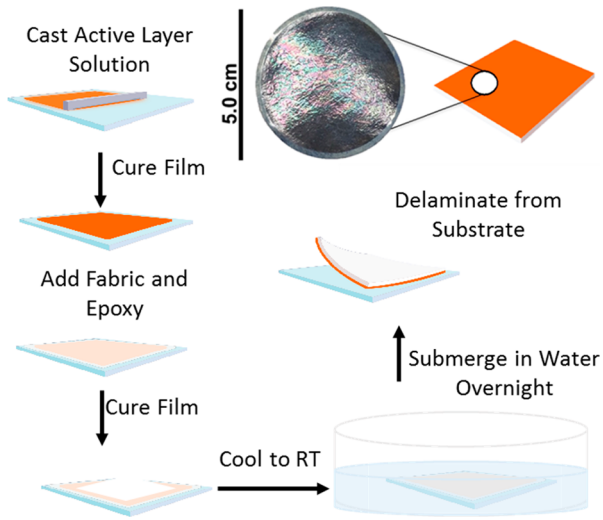

Figure 1. Fabrication of thin-film liftoff (T-FLO) reverse osmosis (RO) membranes. The thin-film interference pattern created by a several-hundred-nanometers-thick active layer can be seen in the top right photograph.

Because the active layer is cast separately from the support, the physical and chemical properties of the active layer can be investigated independently from the entire membrane composite. As long as these techniques are nondestructive, the active layer can be directly fabricated into thin-film composite membranes with the T-FLO technique and studied during operation in a pressurized cell.

RESULTS AND DISCUSSION

When choosing a porous support material to lift-off the active layer, several criteria must be considered:

(1) The support must form strong interactions with the active layer to resist delamination during the lift-off process;
(2) The material must be able to be made into a tunable porous network that is highly permeable; and
(3) The material must be mechanically flexible and robust so it can be handled easily and used under pressurized conditions since RO is performed at 200−800 psi.

After screening several different polymer systems, thermosetting epoxy resins were found to be most suitable for T-FLO membrane fabrication. Cross-linked epoxy networks are known for their high strength and good chemical stability. Their bulk properties can be readily modified by selecting different polyamine hardeners, changing stoichiometric ratios of hardeners to the resin, or adjusting the cure temperature/duration.[21] The highly reactive epoxide groups enable the curing network to covalently bind to functional groups on the active layer (see Figure S2 in the Supporting Information). Furthermore, fabricating porous epoxy membranes can be readily achieved by adding water-soluble polyglycol porogens into the uncured resin solution.[22] After curing, the membrane is submerged into a water bath that serves two functions. The water removes the porogen from the cured epoxy network, forming the porous support membrane, and simultaneously, the water slowly swells the active layer to enable delamination of the entire composite from the underlying substrate.

Figure 2 illustrates the reaction of Bisphenol A digylicyl ether (BADGE) with 4,4′-methylene-bis-cyclohexylamine (MBCA) in the presence of PEG during the curing of the support layer. First, the mixture of monomers reacts to produce linear polymers from the reaction of the epoxides and the diamines to form a resin. The secondary amines and resulting hydroxyl groups react with additional BADGE to form the hardened cross-linked network. The final structure of the cured polymer network using different molecular weight PEGs can be investigated with infrared-attenuated total internal reflection (IR-ATR) spectroscopy (see Figure S5 in the Supporting Information) and X-ray photoelectron spectroscopy (XPS) (see Figure S4 in the Supporting Information). However, differential scanning calorimetry (DSC) shows very similar traces when cycled from 30 °C to 300 °C, indicating that the glass-transition temperature (T_g) of the polymer is not significantly affected. We believe that the differences in the mechanical and transport properties of the epoxy membranes are largely due to the resulting pore macrostructure, as opposed to slight changes in the cross-linking density of the epoxy network (see Figure S6 in the Supporting Information). We have found that the permeability and compaction properties of the epoxy support layer can be readily optimized by changing the ratio of polyethylene glycol (PEG) M_n = 200 (denoted hereafter as PEG200) to PEG M_n = 400 (denoted as PEG400) porogen in the liquid resin. Membranes with larger pores appear opaque when wet, are flexible, and have higher permeabilities, compared to membranes with smaller pores that are transparent and brittle. Figure 3 demonstrates the correlation between control of pore size by porogen composition and control of flux and compaction. In addition, we have observed that these properties are maintained when a dense active layer is present in the composite.

We determined that the effect of the porogen PEG compounds with different molecular weights on the support membrane morphology originated from the density of hydroxyl groups in the porogen. The catalytic effect of various small-molecule alcohols on the kinetics of epoxy network formation is well understood; hydrogen bonding stabilizes the ring opening of epoxides as the resin cures.[23] In our system, a similar effect is achieved with the terminal −OH groups on the PEG porogens used to dissolve the resin and create pores in the cured structure (Figure 2B). A higher density of −OH groups per unit mass of porogen, such as 3.25 g of PEG200, compared to 3.25 g of PEG400, has a larger catalytic effect on

DOI: 10.1021/acs.nanolett.9b01289
Nano Lett. 2019, 19, 5036−5043

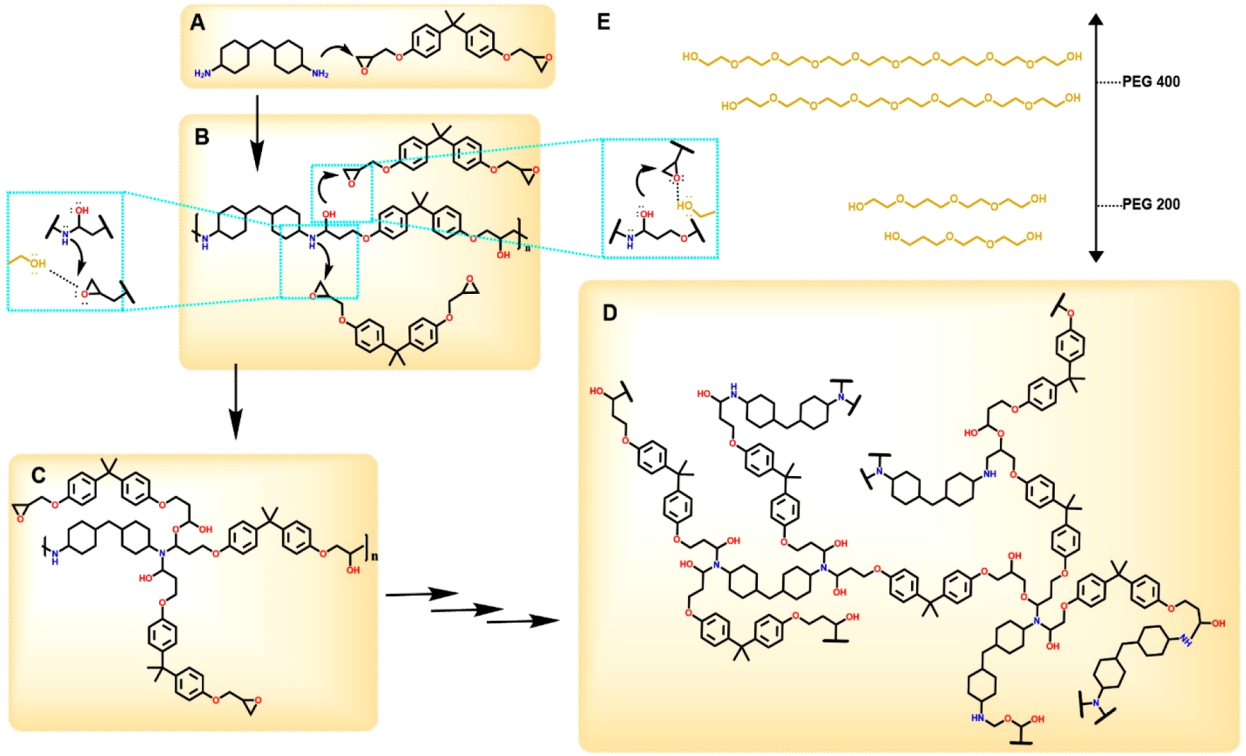

Figure 2. (A) Monomers MBCA (left) and BADGE (right) used for support layers. Tan regions represent PEG porogen. (B) After initial reaction of the monomers to form linear polymers, excess BADGE leads to secondary reactions between epoxy groups and alcohol or secondary amine groups to form branches and cross-links. Insets show role of PEG in stabilizing the ring opening. With these reactions, PEG becomes displaced to form large or small pores. (C) Backbone with BADGE partially reacted. (D) Representation of support layer chemical structure. (E) Primary chemical structures of PEG200 or PEG400 (represented by beige shading within the figure).

the curing rate, i.e., epoxy polymerization and cross-linking. Curing causes phase separation between the porogen and the resin. Consequently, a more rapid phase separation leads to thin pore walls and larger pores. In contrast, fewer terminal −OH groups per unit mass from PEG400 leads to a more-gradual phase separation, resulting in a tighter pore structure with thick pore walls and narrow pores. We confirmed this relationship by removing all −OH groups from the porogen by substituting the PEG porogen with methyl-capped poly(ethylene glycol) dimethyl ether (Me-PEO, M_n = 250). The terminal methyl ether moieties do not interact with the epoxides in the resin, imparting no catalytic activity. When the Me-PEO was solely used as the porogen, only partial curing occurred and a solid film did not form under the same curing conditions. The use of Me-PEO in combination with PEG also did not form a usable membrane film, unless a majority of the porogen blend was PEG (>50 wt %; see Figure S1 in the Supporting Information). Although several liquid PEG porogens could be used from M_n = 100−500), we selected blends of PEG200 and PEG400 as the porogen to demonstrate that the fine-tuning of the density of porogen −OH groups causes significant changes in the final membrane pore structure.

To produce T-FLO composite membranes with comparable permeability to commercial membranes, both the active layer and the support layer must be thin. This can be achieved by casting thin films on glass plates or aluminum sheets using a doctor blade with a fixed height. Here, we demonstrate the T-FLO technique using several different polymers and carbon-based materials to produce membranes for different applications. A major challenge that had to be overcome was curing the epoxy support at a specific height due the change in viscosity of the resin mixture during curing. Our solution to this problem was to create a sandwich structure between two panes of glass using strips of ∼65-μm-thick electrical tape as a spacer to ensure a uniform thickness. Despite fabricating suitable samples for cross-sectional analysis (see Figure S3 in the Supporting Information), the process of separating two panes of glass that were held together by the epoxy resin was arduous. We developed a simpler approach by implementing a thin nonwoven fabric veil that was made of glass, carbon, or polymer fibers to use as a framework to cure the epoxy resin. The liquid epoxy infuses directly into the thin veil, and upon curing, forms a fiber-reinforced plastic film that can be easily handled. Fiber-reinforced plastics are well-known commercially for their lightweight and high strength and are the basis for carbon-fiber composites, body armor, and high-performance sports equipment, and have been implemented extensively in the automotive and aerospace industries.[24] Several materials were considered and screened for the selection of a compatible support fabric. The optimal materials were chemically inert to the epoxide chemistry within the resin, had low thermal expansion coefficients, and were flexible. We observed that nonwoven glass fiber, carbon fiber, and polyester veils with an areal weight of 12 g/m^2 provided the best balance of mechanical and transport properties in the resulting composite membranes.

Once the T-FLO method was developed, we began investigating its use to make composite membranes with active layers that otherwise could not be made using traditional membrane casting techniques.

DOI: 10.1021/acs.nanolett.9b01289
Nano Lett. 2019, 19, 5036−5043

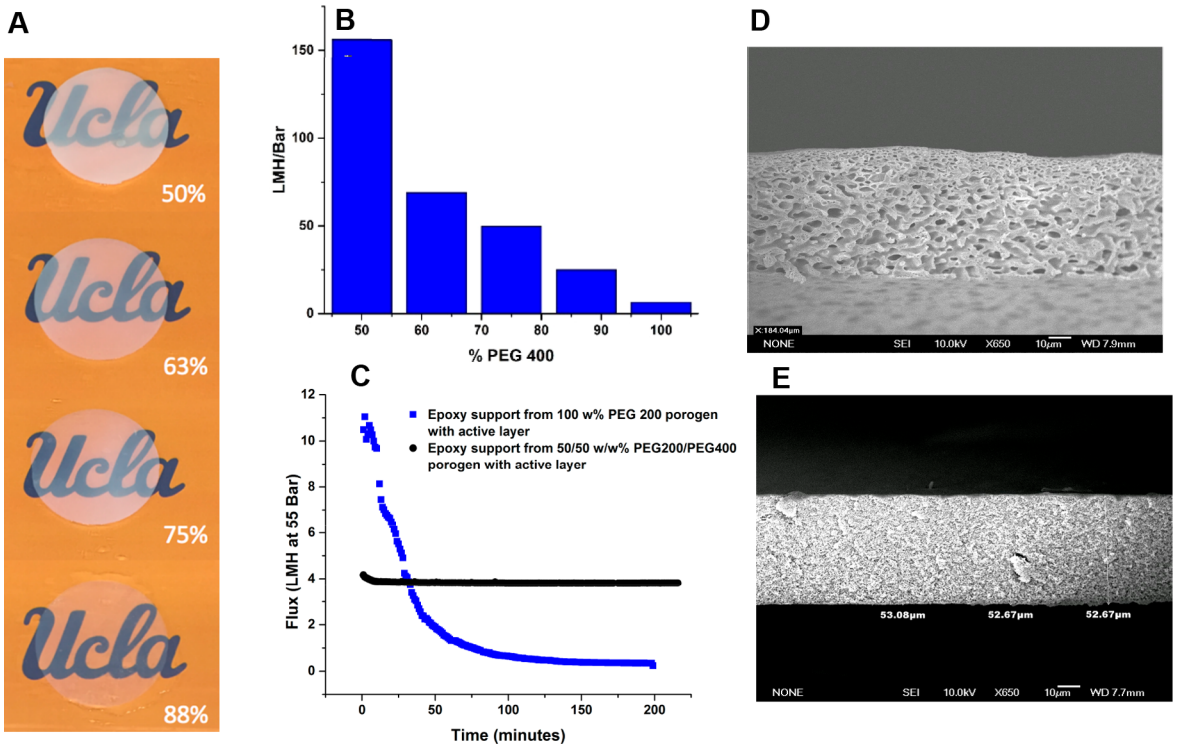

Figure 3. (A) Higher concentrations of porogen PEG400 produces membranes with enhanced density that appear more transparent when wet (the percentage of PEG400 in the porogen mixture is stated in white). (B) Increasing the weight percentage of PEG400 in the porogen mixture produces denser epoxy support membranes that decrease permeability. (C) Denser epoxy support membranes inprove compaction resistance. SEM cross section images show an open pore structure and larger pores are observed in the support made from (D) the 100% PEG200 porogen, and (E) a denser pore structure with smaller pores are observed in the support made from 50/50 wt % PEG200/PEG400 porogen.

Chlorine-Tolerant Reverse Osmosis (RO) Membranes. Pressure-driven reverse osmosis has emerged as the leading technology for desalination of seawater−brackish water, because of its continuous operation, small footprint, and low-energy cost, compared to other desalination technologies. Despite their superior performance, polymeric thin film membranes foul due to organic and biological materials in the feed that adhere to the membrane surfaces. These biofilms restrict the passage of water through the membrane, increasing resistance and lowering efficiency. Chlorination of feedwater is a common way to control the formation and growth of biofilms. However, state-of-the-art thin-film composite membranes are highly susceptible to degradation with even trace amounts of chlorine present in the feed solution. The amide bonds that comprise the backbone of the rejecting layer rapidly hydrolyze, thus compromising the initial high salt rejection of the polyamide membranes.[25,26] Treatment plants must remove virtually all sodium hypochlorite from the feedwater before exposure to the RO membranes, enabling fouling to occur and creating additional steps that increase the cost of desalination.[27,28]

In this work, support membranes were optimized for high-pressure RO by using PEG400 as the porogen, applying a minimal amount of diamine hardener, and selecting carbon fiber as the inert support fabric to lift off the polymeric thin films. This formulation makes for a very dense porous network intended to give added strength and minimize membrane compaction under high pressure (see Figure S7 in the Supporting Information). With T-FLO, we can judiciously select polymers used for the active layer that are tolerant to harsh chemical treatments such as chlorine (for example, polyimides and polybenzimidazoles). Both polyimides and polybenzimidazoles covalently bind to epoxy resin T-FLO supports once glycidyl ether groups in the support resin react with secondary amines in the cured active layer polymer. In the case of polyimides, secondary amines arise due to incomplete cyclization of the polyamic acid precursor when it is cured to form polyimide, whereas in polybenzimidazole, the imidazole functionalities serve as reaction sites. Circular membrane coupons (5 cm in diameter) punched out from flat sheets were tested for salt rejection at 55 bar of applied pressure using a 300-mL, stirred dead-end cell apparatus. Pressure was applied using compressed nitrogen gas. Accelerated chlorine tolerance tests were performed by dipping already-tested coupons into an 8.5% commercial solution of sodium hypochlorite (NaClO) for 5 min. As demonstrated in Figure 4, a T-FLO membrane containing a layered polybenzimidazole/polystyrenesulfonate active layer maintained a high salt rejection of 2000 ppm of NaCl when exposed to sodium hypochlorite, because the polymers used for the active layer have great oxidative stability. In comparison, the salt rejection of a commercial Dow SWXLE membrane substantially decreased due to degradation of the polyamide active layer that is known to rapidly deteriorate when exposed to even trace amounts of sodium hypochlorite.

Organic Solvent Nanofiltration. Organic solvent nanofiltration (OSN) provides a complementary technique or alternative to traditional solvent purification methods (i.e., distillation, chromatography, extraction). Using OSN, desirable solutes can be readily concentrated or waste products can be rejected to purify solvents by passing them through a membrane. Current membranes for OSN are made using

DOI: 10.1021/acs.nanolett.9b01289
Nano Lett. 2019, 19, 5036−5043

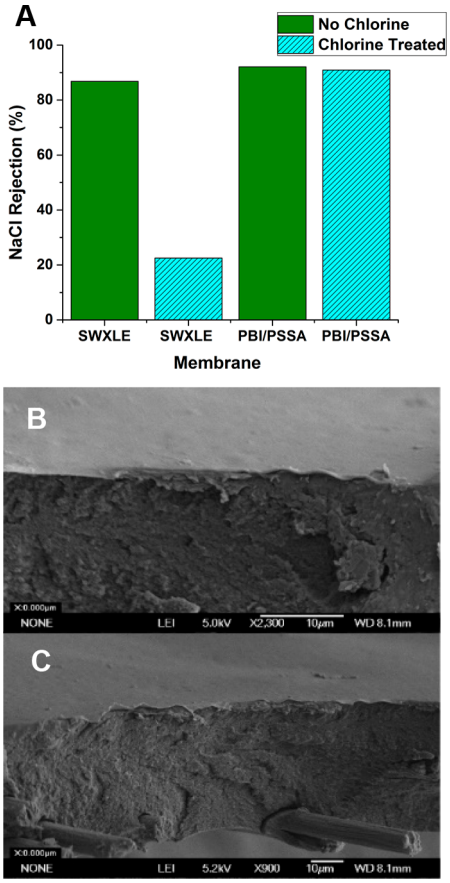

Figure 4. (A) Comparison of PBI/PSSA T-FLO membrane and DOW Filmtec SWLE PA membrane rejection of 2000 ppm of NaCl at 800 psi before and after 5 min of exposure to 8.25% NaClO. (B) T-FLO SEM cross-section showing active layer, epoxy matrix, and carbon fiber at 300× magnification. (C) T-FLO SEM cross-section at 2300× magnification.

traditional membrane fabrication techniques that limit the selection of polymers for the membrane active layers.

Because epoxy-based polymers have good chemical stability and an array of cross-linked or selectively insoluble polymers can be utilized, T-FLO membranes can be tuned for OSN applications. We demonstrate this feasibility by fabricating T-FLO membrane composites and selecting polybenzimidazole (PBI) as the active layer material. PBI is well-known for its chemical stability, stiffness, and toughness at elevated temperatures.[29] Furthermore, Valtcheva et al. have demonstrated that PBI membranes formed using phase inversion exhibit great OSN capability and minimal degradation, even under extreme conditions. However, non-solvent-induced phase inversion offers little control over the active layer thickness. Using the T-FLO technique, the membrane thickness can be precisely controlled by changing the concentration of the casting solution. The epoxy support layer can be tuned independently of the active layer, using T-FLO, which enables the optimization of polybenzimidazole for OSN applications separate from other aqueous separations. To demonstrate the membrane OSN capabilities, a solution of ethanol containing Methylene Blue and a solute was pressurized and passed through a T-FLO membrane (see Figure 5). The membrane rejected ~90% of the dye solute in a single pass, and steady-state permeability was observed at operating pressures up to 300 psi.

Gas Separation. Gas separations can be performed using dense polymeric films, but cryogenic fractionation and adsorption are more common separation techniques, even though they are more energy-intensive processes.[30] Tunable gas separations have been demonstrated previously using polyaniline, but the difficulty in processing polyaniline limits its applications.[31] Polyaniline (PANI) films with graphene oxide (GO, added for improved permeability) were cast on glass plates and dried in a vacuum oven at 80 °C for 36 h. since no additional mass loss was observed with further drying. Afterward, the PANI membrane films were submerged in DI water and separated from their substrates. Figure 6 illustrates how the selectivity for particular gases can be optimized by changing the active-layer film's thickness, thus accentuating the flux difference of CO_2 vs N_2. Processing and handling thinner films (in this case, 500 nm) is made possible using T-FLO. This enables the isolation of physical and chemical parameters when investigating new materials, as well as improve the performance of known materials.

By measuring the pressure difference between the inlet and permeate sides of both epoxy membranes and epoxy membranes with covalently bound PANI active layers, the advantages of T-FLO for gas separation become evident. As shown in Figure S9 in the Supporting Information, the epoxy support does not affect the gas permeability in the presence of the active layer. The PANI film and PANI support membrane were degassed in the membrane cell unit, using a vacuum

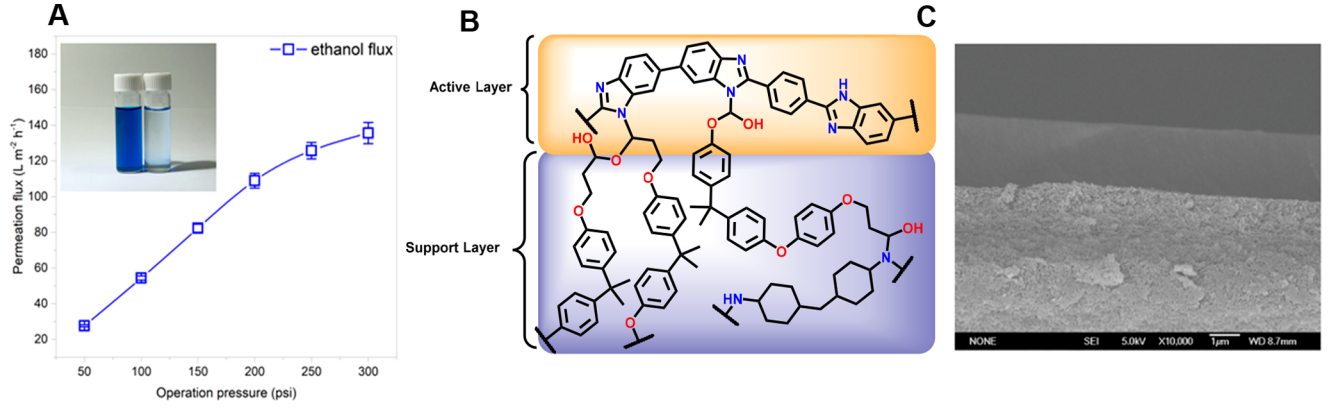

Figure 5. (A) Ethanol flux through a PBI OSN membrane. (B) Schematic of the active layer/support layer interface. (C) SEM image showing the results of a single-pass Methylene Blue dye removal experiment (see inset). SEM cross-section of a PBI OSN membrane at 10 000× magnification.

DOI: 10.1021/acs.nanolett.9b01289
Nano Lett. 2019, 19, 5036−5043

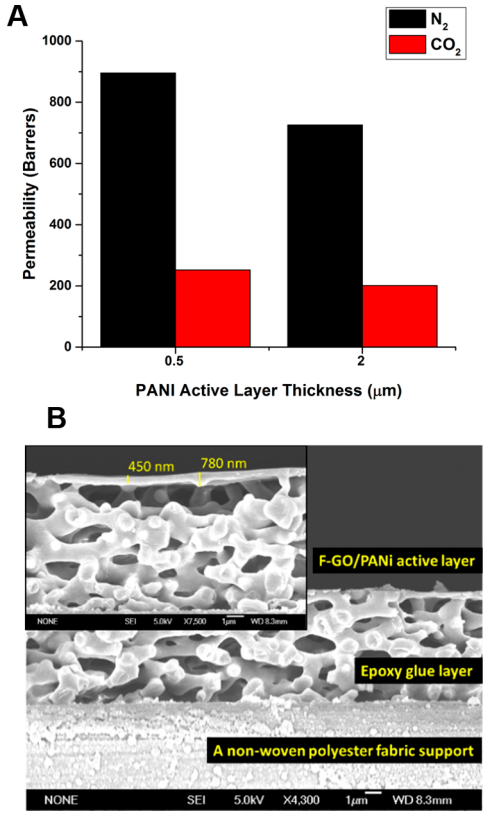

Figure 6. (A) Selectivity data for polyaniline (PANI) thin films with and without a support membrane. (B) SEM image of a sample PANI membrane cross section.

pump at room temperature. The increase in permeation pressure with time was measured using a pressure transducer. The permeability of pure CO_2 and N_2 gases was calculated as

$$P = 10^{10} \times \frac{VL}{P_{\text{permeate}} ART} \times \frac{dp(t)}{dt} \quad (1)$$

where P is the gas permeability (in Barrers, where 1 Barrer = 10^{-10} cm^3(STP)cm/cm^2 s cm Hg), P_{permeate} the upstream pressure (cm Hg), dp/dt the steady-state permeate-side pressure increase (cm Hg/s), V the calibrated permeate volume (cm^3), L the membrane thickness (cm), A the effective membrane area (cm^2), T the operating temperature (K), and R the gas constant (R = 0.278 cm^3 cm Hg/cm^3(STP) K).

The ideal selectivity (α) is determined from the ratio of permeability coefficients (eq 2):

$$\alpha_{A/B} = \frac{P_A}{P_B} = \frac{P_{CO_2}}{P_{N_2}} \quad (2)$$

where P_A and P_B refer to the permeability coefficients of the pure gases CO_2 and N_2, respectively. Figure S9 in the Supporting Information shows the comparison of the CO_2 permeance of the membranes with and without the epoxy layer. The pure CO_2 and N_2 permeance were measured at a feed pressure of 7 psi (0.048 MPa). The CO_2 permeability of the PANI film membrane (without the epoxy layer) is only slightly higher than that measured for the PANI support membrane alone. However, the difference in CO_2 and N_2 permeance was insignificant, which indicates that CO_2 and N_2 permeance were not affected by the epoxy layer because its large pores do not reduce the penetration of the gases.

CONCLUSIONS

Here, we introduce T-FLO as a novel technique to fabricate thin-film composite membranes for reverse osmosis, organic nanofiltration, and gas separation. Because the active layer is cast separately from the porous support, a variety of active layer materials can be selected, specific to each application. In addition, the ability to cast the active layer separate from the support membrane enables the ability to control the thickness of the active layer and perform post-treatments solely on the active layer without consideration of chemical or thermal stability of the porous support. We have developed a fiber-reinforced epoxy support that, upon curing, simultaneously forms a porous network while covalently binding to the active layer. The pore size and permeability of the support is well controlled through the use of a water-soluble PEG porogen that is removed during the thin film lift-off process in an aqueous bath solution. With gas permeation membranes, the support does not restrict the permeation of gases through the membrane. We believe that the T-FLO membranes will enable the use of exciting new polymers, carbon materials, and metal–organic frameworks in the next generation of membranes for separation applications.

MATERIALS AND METHODS

Active layer polymer solutions were prepared by dissolving the selected polymer(s) in a suitable solvent to form a viscous solution. The solutions were centrifuged at 13 000 rpm to remove agglomerates and the supernatant cast onto clean glass plates using a doctor blade with a fixed height (7.62 μm wet film thickness, GardCo, Inc.). A uniform film formed upon evaporation of the solvent. For higher-boiling solvents, gentle heat can be applied underneath the glass substrate to aid in evaporation. Higher curing temperature treatments can be performed for cyclization of prepolymers or cross-linking reactions.

To prepare the resin for the microporous support membrane, 280 mg of 4,4′-methylenebis(cyclohexylamine) and 3.25 g of polyethylene glycol (PEG) of a specific average molecular weight (200 g/mol, 400 g/mol or a mixture of both) was charged to a scintillation vial and stirred with a magnetic stir bar until the diamine was fully dissolved. 1.0 g of Bisphenol A diglycidyl ether (Sigma–Aldrich) was then added to the solution with stirring at 700 rpm for 90 min to promote linear polymerization and achieve full dissolution. The solution was then degassed under reduced-pressure and poured on top of a precast active layer film/glass substrate on top of a level hot plate. A 11 cm × 14 cm nonwoven glass, polyester, or carbon fiber fabric sheet was placed on top of the active layer to absorb the epoxy solution and reinforce the cured membrane. Uniform heat was applied through a custom-built hot-plate (Wenesco, Inc.) for 3 h, to cure the epoxy solution into a porous film. Once cured, the glass plate supporting the membrane was allowed to cool and placed into a deionized (DI) water bath to delaminate the membrane from the glass substrate and remove the porogen. NaCl can be added to the solution to accelerate delamination by increasing the swelling of the active layer. The membranes were stored in DI water or NaCl solution before further use.

Reverse Osmosis (RO) Active Layer. Desalination membranes were made by casting thin films of polystyrene sulfonic acid in water (PSSA, Sigma–Aldrich, 1% w/v) onto clean glass substrates. Gentle heating was applied to evaporate

DOI: 10.1021/acs.nanolett.9b01289
Nano Lett. 2019, 19, 5036–5043

the solvent, followed by casting of a PBI solution in DMAc and THF directly atop the PSSA layer. THF was used as a cosolvent to encourage faster solvent evaporation that enabled higher film quality, because of a reduction in the number of defects that can form upon prolonged drying or rapid evaporation of a higher boiling solvent. Acid−base interactions occurred upon contact, followed by curing for 4 h at 180 °C to induce cross-linking. A carbon fiber veil (12 g/m^2) was used in the support membrane. 100% PEG400 was used as the support resin porogen. Rejection of salt and flux of water through RO membranes was performed in a 300 mL, dead-end, stirred cell pressurized using compressed nitrogen gas.

Organic Solvent Nanofiltration (OSN) Active Layer. For organic solvent nanofiltration membranes, a commercial solution of Celazole polybenzimidazole (Performance Products, Inc. (PBI)), 10% in dimethylacetamide (DMAc) was diluted and then cast onto a glass substrate and heated to 60 °C to remove solvent. A nonwoven glass fiber veil (12 g/m^2) was used as the supporting fabric. 100% PEG400 was used as the support resin porogen. Rejection of Methylene Blue and the flux of ethanol through OSN membranes was performed in a 300 mL, dead-end, stirred cell pressurized using compressed nitrogen gas.

Gas Separation Active Layer. Polyaniline (PANI) composite films were made by casting a thin film of PANI-graphene oxide (0.2 wt % GO and 0.8 wt % PANI in NMP) onto a glass plate, followed by solvent evaporation. In all cases, film composition and solvent could be tuned for optimal film quality. A nonwoven polyester fiber veil (12 g/m^2) was used in the support membrane. 100% PEG200 was used as the support resin porogen.

■ ASSOCIATED CONTENT

Supporting Information

The Supporting Information is available free of charge on the ACS Publications website at DOI: 10.1021/acs.nanolett.9b01289.

Preparaton of epoxy resin and noncomposite epoxy membranes (Figure S1); preparation of epoxy prepreg solutions and curing of the porous support to form composite membranes (Figure S2); methyl-capped poly(ethylene oxide) experiments (Figure S3); preparation of samples for SEM observation (Figure S4); notes on the types of nonwoven fabric reinforcement (Figure S5); schematic of active layer−support layer bonding (Figure S6); cross-sectional images of non-fiber-reinforced epoxy membranes (Figure S7); X-ray photoelectron spectroscopy analysis of epoxy membranes (Figure S8); infrared spectroscopy analysis of epoxy membranes (Figure S9); differential scanning calorimetry of epoxy membranes (Figure S10); sample of DI water flux through PBI RO membrane at variable pressures (Figure S11); and gas separation control experiments (Figure S12) (PDF)

■ AUTHOR INFORMATION

Corresponding Author

*Tel.: (310) 825-5346. E-mail: kaner@chem.ucla.edu.

ORCID

Mackenzie Anderson: 0000-0002-7605-2558

Dayong Chen: 0000-0002-6226-3370

Gaurav Sant: 0000-0002-1124-5498

Richard B. Kaner: 0000-0003-0345-4924

Present Address

[▽]607 Charles E. Young Dr. E, Los Angeles, CA 90095, USA.

Author Contributions

[⊥]These authors contributed equally to this work.

Notes

The authors declare no competing financial interest.

■ ACKNOWLEDGMENTS

This work is supported by the U.S./China Clean Energy Research Center for Water-Energy Technologies (CERC-WET) (R.B.K. and G.S.), the UCLA Grand Challenges (R.B.K. and G.S.), the National Science Foundation Grant DGE-1735325 (M.A.), and the Dr. Myung Ki Hong Endowed Chair in Materials Innovation (R.B.K.). We thank Technical Fiber Products for their generous donation of the nonwoven fabrics used in this work.

■ REFERENCES

(1) Lee, K. P.; Arnot, T. C.; Mattia, D. *J. Membr. Sci.* **2011**, *370* (1−2), 1−22.

(2) Loeb, S. The Loeb−Sourirajan Membrane: How It Came About. In *Synthetic Membranes*; Turbak, A. F., Ed.; ACS Symposium Series, Vol. *153*; American Chemical Society: Washington, DC, 1981; pp 1−9.

(3) Reid, C. E.; Breton, E. J. *J. Appl. Polym. Sci.* **1959**, *1* (2), 133−143.

(4) Geise, G. M.; Paul, D. R.; Freeman, B. D. *Prog. Polym. Sci.* **2014**, *39* (1), 1−42.

(5) Wang, J.; Dlamini, D. S.; Mishra, A. K.; Pendergast, M. T. M.; Wong, M. C.Y.; Mamba, B. B.; Freger, V.; Verliefde, A. R.D.; Hoek, E. M.V. *J. Membr. Sci.* **2014**, *454*, 516−537.

(6) Petersen, R. J., Cadotte, J. E., Porter, M. E., Eds. *Handbook of Industrial Membrane Technology*; Noyes Publications, Park Ridge, NJ, 1990; p 307.

(7) Petersen, R. J. *J. Membr. Sci.* **1993**, *83* (1), 81−150.

(8) Nowbahar, A.; Mansard, V.; Mecca, J. M.; Paul, M.; Arrowood, T.; Squires, T. M. *J. Am. Chem. Soc.* **2018**, *140*, 3173−3176.

(9) Chai, G.-Y.; Krantz, W. B. *J. Membr. Sci.* **1994**, *93*, 175−192.

(10) Prakash Rao, A.; Desai, N.V.; Rangarajan, R. *J. Membr. Sci.* **1997**, *124*, 263−272.

(11) Prakash Rao, A; Joshi, S.V; Trivedi, J.J; Devmurari, C.V; Shah, V.J *J. Membr. Sci.* **2003**, *211*, 13−24.

(12) Song, Y.; Sun, P.; Henry, L.; Sun, B. *J. Membr. Sci.* **2005**, *251*, 67−79.

(13) Roh, I. J.; Greenberg, A. R.; Khare, V. P. *Desalination* **2006**, *191*, 279−290.

(14) Ghosh, A. K.; Jeong, B.-H.; Huang, X.; Hoek, E. M. V. *J. Membr. Sci.* **2008**, *311*, 34−45.

(15) Liu, M.; Yu, S.; Tao, J.; Gao, C. *J. Membr. Sci.* **2008**, *325*, 947−956.

(16) Jin, Y.; Su, Z. *J. Membr. Sci.* **2009**, *330*, 175−179.

(17) Xie, W.; Geise, G. M.; Freeman, B. D.; Lee, H.-S.; Byun, G.; McGrath, J. E. *J. Membr. Sci.* **2012**, *403−404*, 152−161.

(18) Klaysom, C.; Hermans, S.; Gahlaut, A.; Van Craenenbroeck, S.; Vankelecom, I. F. J. *J. Membr. Sci.* **2013**, *445*, 25−33.

(19) Hoek, E. M. V.; Bhattacharjee, S.; Elimelech, M. *Langmuir* **2003**, *19*, 4836−4847.

(20) Hong, S.; Kim, I.-C.; Tak, T.; Kwon, Y.-N. *Desalination* **2013**, *309*, 18−26.

(21) Jin, F.-L.; Li, X.; Park, S.-J. *J. Ind. Eng. Chem.* **2015**, *29*, 1−11.

(22) Kawaguchi, Y.; Hiro, A.; Harada, N.; Hayashi, O.; Mizuike, A.; Ishii, K. U.S. Patent No. 0174723, July 21, 2011.

(23) Shechter, L.; Wynstra, J.; Kurkjy, R. P. *Ind. Eng. Chem.* **1956**, *48* (1), 94−97.

(24) Meier, U. *Constr. Build Mater.* **1995**, *9* (6), 341−351.

DOI: 10.1021/acs.nanolett.9b01289
Nano Lett. 2019, 19, 5036−5043

(25) Barassi, G.; Borrmann, T. *J. Membr. Sci. Technol.* **2012**, *02* (02), 2−4.
(26) Do, V. T.; Tang, C. Y.; Reinhard, M.; Leckie, J. O. *Environ. Sci. Technol.* **2012**, *46* (2), 852−859.
(27) Jamaly, S.; Darwish, N. N.; Ahmed, I.; Hasan, S. W. *Desalination* **2014**, *354*, 30−38.
(28) Isaias, N. P. *Desalination* **2001**, *139* (1−3), 57−64.
(29) Valtcheva, I. B.; Kumbharkar, S. C.; Kim, J. F.; Bhole, Y.; Livingston, A. G. *J. Membr. Sci.* **2014**, *457*, 62−72.
(30) Liu, C.; Greer, D. W.; O'Leary, B. W. *ACS Symp. Ser.* **2016**, *1224*, 119−135.
(31) Anderson, M. R.; Mattes, B. R.; Reiss, H.; Kaner, R. B. *Science* **1991**, *252* (5011), 1412−1415.

DOI: 10.1021/acs.nanolett.9b01289
Nano Lett. 2019, 19, 5036−5043